Received May 27, 2019, accepted June 11, 2019, date of publication June 17, 2019, date of current version July 2, 2019.

Digital Object Identifier 10.1109/ACCESS.2019.2923357

Detection of Multiple Maneuvering Extended Targets by Three-Dimensional Hough Transform and Multiple Hypothesis Tracking

BO YAN[1], NA XU[2], GUANGMIN WANG[1], SHENG YANG[1], AND L. P. XU[1]
[1]School of Aerospace Science and Technology, Xidian University, Xi'an, China
[2]School of Life Sciences and Technology, Xidian University, Xi'an, China

Corresponding author: Bo Yan (boyan@xidian.edu.cn)

This work was supported in part by the National Natural Science Foundation of China under Grant 61701383, and in part by the Natural Science Basic Research Plan in Shaanxi Province of China under Grant 2018JQ6100.

ABSTRACT Existing extended target probability hypothesis density (ET-PHD) filters are insufficient in tracking weak extended targets. Hough transform-based track-before-detect methods are designed to detect the weak targets in a straight-line constant-velocity model. Therefore, this paper presents a novel method for detecting and tracking multiple maneuvering weak extended targets by a 3-dimensional Hough transform (3DHT) and multiple hypothesis tracking (MHT). The proposed method consists of two stages. In stage 1, the measurements in multiple scans are partitioned into overlapped time windows. The tracklets in each window can be detected by the 3DHT. In stage 2, the tracklets are associated to get the entire trajectories by the MHT. The tracklets of weak targets can be detected by the 3DHT in stage 1. Association in stage 2 is designed to detect maneuvering targets. Some false alarm tracklets could be built in stage 1. However, the false alarm tracklets are independent and unlikely to form a sequential trajectory in stage 2. Merely, the trajectories whose target likelihood ratio larger than a detection threshold can be confirmed as a target. Both the real data and the synthetic data are performed with the proposed approach and several existing algorithms. The result infers that the proposed approach is superior to the others with much less prior information that is necessary.

INDEX TERMS Extended target tracking, weak target detection, maneuvering target tracking, Hough transform, multiple hypothesis tracking.

I. INTRODUCTION

Multiple target tracking is an essential requirement for surveillance systems. A fully automatic tracking algorithm must be able to deal with an unknown number of targets, unknown target initiation and termination times, false measurements and possibly time-varying target trajectory behavior [1]. Multiple target track (MTT) is always a challenging problem for two reasons. The first one is the quantity and state of targets are generally unknown a priori and time-varying. Secondly, the indication on the source of each measurement is not known. Meanwhile, for the present of clutter, a measurement may originate from random clutter and also from targets. Recently, MTT problem becomes more sophisticated for the increased resolution of modern radars. The high resolution allows the target to be found in several pixels of radar video data and then the radars are able to receive more than one detection per time step from different corner reflectors of a single target. Rather than categorizing the target as a point, the target in this work is regarded as an extended target. More than one points may be generated by an extended target. This work is devoted to addressing the problem of multi-extended target tracking and detection.

In the past of a few years, various algorithms have been developed to address the multiple extended target track (METT) problem. The most popular and widely used approach is the probability hypothesis density (PHD) filter based methods [3], [4]. Following the random finite set theory

The associate editor coordinating the review of this manuscript and approving it for publication was Mehmet Alper Uslu.

This work is licensed under a Creative Commons Attribution 3.0 License. For more information, see http://creativecommons.org/licenses/by/3.0/

of Ronald Mahler [5], the measurements (points) are partitioned into sets before the iteration of the PHD filter. Each set regards the measurements of one extended target in one scan. Then, the PHD filter could simultaneously associate all measurement sets with all tracks, rather than attempting to enumerate and rank a list of possible measurement-to-track associations in [1]. Correct partitions are significant to achieve remarkable tracking performance. Therefore, improved measurement partition approaches are also developed [6]–[8]. However, the number of possible partitions grows very large as the number of measurements increases. Even only a subset of all possible partitions is considered, it brings huge computation with alternative partitioning. Meanwhile, the PHD based filters only use the data in the current scan. Weak targets in a cluttered environment are hard to be detected for the measurement noise and false alarm. Therefore, in our former work [3], a 3DHT-TBD (3-Dimensional Hough Transform based Track-Before-Detect) which has low sensitivity to a local fault and outstanding ability in suppressing noise and clutters is developed in [9]. The 3DHT-TBD is able to perform target detection, data association, track initiation, and track maintenance at the same time in an intense clutter environment. Compared with the PHD filters, better tracking performance can be achieved. However, shortcoming still exists. The HT [9], [10] is designed to extract straight-line target trajectories in the Cartesian data and the targets in [9] follow a straight-line constant-velocity mobility model. The detection rate and tracking precision can be greatly deteriorated when the target is maneuvering. To address the issue of extended maneuvering target detection and tracking, a grey wolf optimization [11] based track before detect (GWO-TBD) method is developed in [12]. A weak and maneuvering extended target in a cluttered environment can be well detected. However, some limitations still exist. The GWO-TBD only cope with one target at a time. In multiple targets tracking scenarios, the targets can be detected one by one only when the targets are far away from each other. Its performance would be deteriorated if several maneuvering extended targets are closely distributed because several optimal solutions exist in this scenario simultaneously. To deals with the problem of tracking the two-dimensional direction-of-arrivals (DOAs) of multiple moving targets with crossover points on their trajectories, we propose a new computationally efficient cross-correlation based 2-D DOA estimation with automatic pair-matching (CODEC) method in [13], [14]. Multiple maneuvering targets can be well tracked by joint integrated probabilistic data association (JIPDA) based methods [15], [16] and Multiple hypotheses tracking MHT based methods [17], [18]. However, the point-to-point association in [15]–[18] are designed for non-extended targets. Quite a few redundancy trajectories would be built when we use the JIPDA [15], [16] or the MHT [17], [18] directly.

Therefore, a method to detect and track multiple closely distributed weak and maneuvering extended target in a cluttered environment is proposed in this work. The 3-dimensional Hough transformation [2] and multiple hypothesis tracking algorithm is utilized to ensure the ability to detect weak target and maneuvering target respectively. Different with the point-to-point association based MHT in [17], [18], the multiple hypothesis tracking algorithm in this work bases its principle of tracklet-to-tracklet association. Meanwhile, the track-before-detect technology is also applied for taking full advantages of multiple scans (including the current scan and some past scans). Therefore, the proposed approach is providing the name ''3DHT-MHT (3-Dimensional Hough Transform and Multiple Hypothesis Tracking) method''. The input of the 3DHT-MHT method is the 3-dimensional measurement points (2-dimensional positional information and its measuring time) of several successive scans.

The 3DHT-MHT consists of two stages. The first stage is detecting the tracklets by the 3-Dimensional Hough Transform in overlapped time windows. Each window contains the measurements of several scans. In the second stage, the tracklets of different windows are associated to form the entire trajectory of each target with the multiple hypothesis tracking algorithm. The proposed approach is superior to the existing methods in four aspects.

Firstly, the points of multiple scans are involved in target detection. The TBD framework is beneficial to weak target detection. Secondly, for the tracklets association in the second stage, maneuvering targets can be also detected. Thirdly, the idea of the Hough Transform is to make the infinite space of all possible lines finite by a discretization of the parameter space and to let each point ''vote'' for all lines to which it belongs in this parameter space [2]. Therefore, partitioning the measurements into sets [3], [4] and association between points in [15]–[18] are avoided. Computational risks are also avoided in multi-track situation. Fourthly, extended target and non-extended target can be detected in the 3DHT simultaneously.

The remainder of the work is organized as follows. Section II defines the models and problems. Section III embeds the extended tracking problem into 3DHT and MHT algorithm. Also, in this section, the detailed description and implementation of the 3DHT-MHT would be presented. To compare the performance of the existing approaches and the proposed method in detail, Section IV demonstrates the effectiveness through the real data of an air surveillance radar and Monte Carlo simulations. Section V draws conclusions.

II. MODELS

A. PRELIMINARIES

It assumes that the extended targets are randomly distributed in an x–y plane. We use N_k to denote the number of targets at k scan. The i^{th} extended target state at k^{th} scan is defined as the triple $\boldsymbol{\xi}_k^i = (\gamma^i, \boldsymbol{x}_k^i, \boldsymbol{X}_k^i)$ [19]. Firstly, the random variable $\gamma^i > 0$ is the measurement rate that describes how many measurements the target, on average, generates per time scan. Secondly, $\boldsymbol{x}_k = (\boldsymbol{p}_k^i, v_k^i, \alpha_k^i)^{\mathrm{T}} \in \mathbb{R}^4$ is the kinematic state. $\boldsymbol{p}_k^i$ describes the target's position where $\boldsymbol{p}_k^i = (x_k^i, y_k^i)$. v_k^i denotes the velocity and α_k^i represents the course of

the target. Finally, $\boldsymbol{X}_k^i$ is the extension of the target and it describes the target's size and shape. The dynamic models and sensor measurement processes related to the state of target ξ_k^i at k^{th} scan are given by Eq.(1) and Eq.(2) respectively.

$$\boldsymbol{\xi}_{k+1}^i = F(\boldsymbol{\xi}_k^i, \sigma) \tag{1}$$

$$\{z\}_k^i = H(\boldsymbol{\xi}_k^i, \omega) \tag{2}$$

where $F(\bullet)$ is the state propagation function and H $(\bullet)$ is the measurement function. Process noise σ and measurement noise ω are zero mean, white and uncorrelated Gaussian noise sequences. The detailed expression of Eq.(1) and Eq.(2) can be found in [8]. The measurement is the detection obtained by a detector such as the constant false alarm rate (CFAR) [20] from the radar video data [21]. In Eq.(2), $\{z\}_k^i$ denotes the measurements of thei^{th} extended target at k^{th} scan. The set of measurements generated by clutter is denoted by $\{z\}_k^0$. The set of measurements $\boldsymbol{Z}_k$ obtained at time k is the collection of measurements generated by targets and clutters. However, indication on the source of each measurement is unknown. Each measurement z_k usually consists of a kinematic (position) measurement component $(x_k^i,\ y_k^i)$ and a time stamp records the received time t_k^i.

$$\begin{aligned}\boldsymbol{Z}_k &= \{z\}_k^1 \cup \ldots \cup \{z\}_k^{N_k} \cup \{z\}_k^0 \\ &= \{z_k^j | j = 1, \ldots, |\boldsymbol{Z}_k|\} \\ &= \{(x_k^j, y_k^j, t_k^j) | j = 1, \ldots, |\boldsymbol{Z}_k|\}\end{aligned} \tag{3}$$

The number of elements in $\{z\}_k^i$ is usually assumed follows a Poisson distribution [22]. The set of all the measurements in a time series is denoted by $\boldsymbol{Z}^K$, $\boldsymbol{Z}^K = \{\boldsymbol{Z_k}\}_k = 1^K$. And the input of the 3DHT-MHT is exactly the points set $\boldsymbol{Z}^k$.

B. PROBLEM STATEMENT

TBD algorithm is a method to improve the detection of weak targets by integrating their signal returns over multiple consecutive scans, i.e. estimate the state of extended targets at each scan ξ by measurements set $\boldsymbol{Z}^K$. The optimal estimation which has a maximum likelihood is:

$$\boldsymbol{\xi}_{\text{T}} = \arg\max P(\boldsymbol{\xi}|\boldsymbol{Z}^K); \quad \boldsymbol{\xi} = \{\boldsymbol{\xi}_k\}_{k=1}^K;\ \boldsymbol{\xi}_k = \{\boldsymbol{\xi}_k^i\}_{i=1}^{N_k} \tag{4}$$

$\boldsymbol{\xi}$ and $\boldsymbol{\xi}_k$ represent the trajectories and the state of the targets in k^{th} scan respectively. For the enormity of the solution space of $\boldsymbol{\xi}$, the estimating of optimal solution $\boldsymbol{\xi}_{\text{T}}$ is a tough issue. Three branches of strategies have been developed for this issue.

The first branch is PHD filter based approaches [3]–[5], before the iteration of the PHD filter. the measurements of each scan are clustered into sets, each set is the measurements generated by the same source, every set of every partition are utilized to update the state of each target [23]. Considering all possible partitions, PHD has a quadratics growth in computation with a linear increase in the number of measurements. Simplification in the algorithm carries an inevitably decrease in performance. Meanwhile, our former work [9] infers that PHD filter is sensitive to the measurement noise and false alarm rate. And it often failed to track the targets when the targets merely generate few measurements. Quite a few false trajectories would be also built in a high false alarm rate scenario.

The second branch is associating the points of the same target by JIPDA [15], [16] or MHT [17], [18]. However, the measurement sets are associated to form the trajectory of an extended target, rather than associating the points directly in the JIPDA [15], [16] or MHT [17], [18]. For taking full benefits of multiscan, some multiscan joint probabilistic data association (mscan-JPDA) approaches [1] are also available. All possible hypotheses regarding target and track to measurement set associations are formed in these methods. Exponential growth of computational expense would arise when we exhaustively list all possible assignments.

In the above two branches, distance partitioning [3] is usually utilized to partition the points. Alternative distance partitioning can be obtained by multiple distances. The partition result of i^{th} distance partitioning can be represented by $\boldsymbol{S}_k^{i,1}, \boldsymbol{S}_k^{i,2}, \ldots, \boldsymbol{S}_k^{i,M_k^i}$. The quantity of alternative partitions is represented by M_k. Then, it has:

$$\boldsymbol{Z}_k = \boldsymbol{S}_k^{i,1} \cup \boldsymbol{S}_k^{i,2} \cup \ldots \cup \boldsymbol{S}_k^{i,M_k^i}; \quad i = 1, \ldots M_k \tag{5}$$

$$\begin{aligned}\boldsymbol{S}_k^{i,j} &= \{z_k^{i,j,n}, n = 1, \ldots, \left|\boldsymbol{S}_k^{i,j}\right|\} \\ &= \{(x_k^{i,j,n}, y_k^{i,j,n}, t_k^{i,j,n}), n = 1, \ldots, \quad \left|\boldsymbol{S}_k^{i,j}\right|\}\end{aligned} \tag{6}$$

where $z_k^{i,j,n}$ means n^{th} point in j^{th} set under i^{th} partitioning distance at kth scan. M_k^i denotes the number of sets if the measurements are partitioned by i^{th} distance in k^{th} scan. Meanwhile, the quantity of partition in this scan is represented by M_k, it also means the quantity of partition distance. The alternative distance partitioning can be illustrated by figure 1a. The measurements of k^{th} scan (green points) can be clustered into two sets with distance 1 and three sets with distance 2. It means that the M_k equals to 2 in figure 1a. The partition 1 and partition 2 regard the points partition results with distance 1 and distance 2 respectively. The d_1 represents the distance between point A and point B. The two points belong to the same set ${\boldsymbol{S}_{k-2}}^{2,1}$ in partition 2 because the distance d_1 is smaller than distance 2. The distance between point C and point D is d_2. The d_2 is larger than the distance 2. Therefore, point C and point D belong to different sets in partition 2. Meanwhile, the d_2 is smaller than distance 1. So, the point C and point D belong to the same set ${\boldsymbol{S}_{k-2}}^{1,1}$ in partition 1. As to the point D and point E, the distance d_3 is larger than the distance 1. Therefore, the point D and point E always belong to the different sets in the partition 1 and partition 2. The points originated from two extended targets can be represented by the measurement sets in figure 1b. $\emptyset$ means an empty set, i.e. no measurements are generated by the target in this scan.

Theoretically, the above methods require all possible partitions of the current measurement set for its update and association. However, the number of possible partitions grows very large as the number of measurements increases.

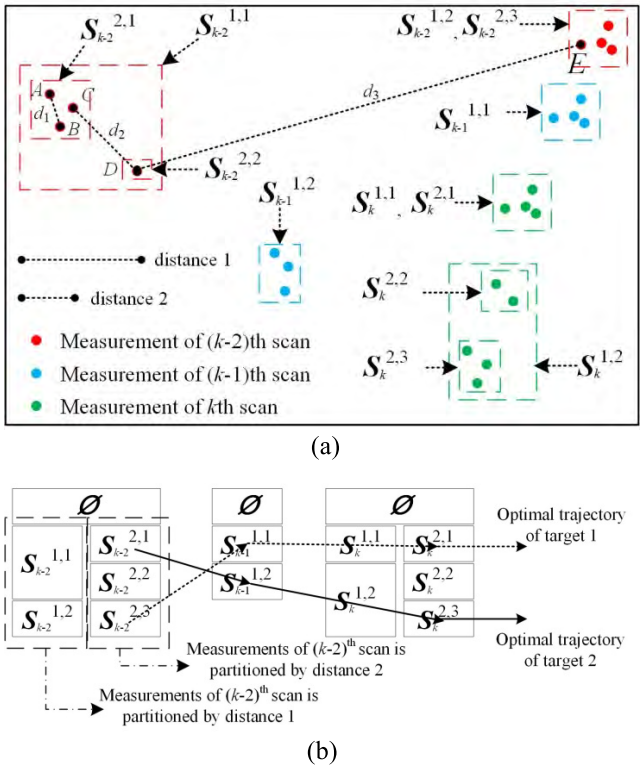

FIGURE 1. (a) Diagram of alternative distance partitioning. (b) Optimal measurement sets of two extended targets.

The computation of PHD filter, MHT and JIPDA would be dramatically increased. Various improved approaches have been developed to keep the number of branches under control in multiple non-extended targets (point targets) tracking, such as the K-best multiple hypothesis tracker [24]. Meanwhile, in our former work [12], one single maneuvering extended target can be well detected by associating the measurement sets directly and the GWO [11] is utilized to decrease the computation. However, the MHT or JIPDA are rarely utilized in multiple extended targets tracking for the hugeous computation.

The third branch is the HT based approaches, including the 3DHT-TBD [9] and 4DHT [10] based methods. Measurement partitioning is avoided because each measurement ''vote'' for all the potential trajectories. The voting process is done in an iterative way by selecting the trajectory with the most votes and removing the corresponding measurements in each step until no trajectories can be detected. However, these methods are designed to detect the non-maneuvering targets, i.e. both the velocity and course of the target are constants. Reference [12] infers that, the performance of the original PHD filter [3] and HT based methods [9], [10] would be greatly deteriorated when targets are maneuvering.

Above discussion infers that all the existing approaches have their own shortcomings. To detect multiple extended maneuvering targets under various severe measurement conditions, the measurements of each extended target should be found out at first. And then the state of each extended target in each scan can be estimated independently. This is exactly what the 3DHT-MHT-TBD is proposed for.

III. HOUGH TRANSFORM & MULTIPLE HYPOTHESIS BASED TRACKING ALGORITHM

A. INTROUDCTION OF THE 3DHT-MHT

The 3DHT-MHT consists of two stages. The first stage is the 3D Hough transform. The input of this stage is the 3-dimensional points of several successive scans. The 3DHT is applied here, rather than the 4DHT, for efficiency because far more voting cells in 4DHT make it time-consuming. However, the points are not fed to the 3DHT at once. As is presented in figure 2a, a sliding window containing the points of a few scans is defined. The points in each sliding window are processed by the 3DHT independently. The trajectories obtained in each sliding window are called ''tracklet'' here. The points of an extended target are distributed near the trajectory of the target. The trajectory in a sliding window can be approximate to a straight line in a 3-dimensional Cartesian space, i.e. X-axis, Y-axis and time-axis. A 3-dimensional accumulator array whose cell representing one set of three parameters from the discretized parameter space is built in the 3DHT. Each set of parameters corresponding to a 3D straight line. Each point would vote for all the lines to which it might belong in this parameter space. Then, backtrace the 3D-line corresponding to the highest voted cell. The tracklet of the targets in a sliding window can be detected iteratively. In figure 2a, $\boldsymbol{T}_k$ is the set of tracklets in sliding window W_k. The output of this stage is the tracklet sets in each scan.

The second stage is associating the tracklets of sliding windows to form the integrated trajectory. Different with the point-to-track association or point-to-point association in traditional MHT approaches, tracklets of the same target are associated, i.e. track-to-track association. The track-to-track version of MHT is presented in figure 2b. Γ_n represents the hypothesis obtained in the n^{th} iteration. All possible associations are listed and the best global hypothesis is selected as the generation of hypothetical trajectories. Each track hypothesis is associated with a track score, which is typically defined as a likelihood ratio between the true target hypothesis probability and false alarm hypothesis probability. Then, to keep the number of branches under control, a track is immediately deleted if its score is below the lower threshold. After merging the similar trajectories, the trajectories whose score exceeds the upper threshold are confirmed as targets. The track whose score falls between the upper and lower thresholds is still tentative and is required to be further tested in the next iteration. Then, the confirmed trajectories are smoothed to acquire more accurate trajectories. The set of the smoothed trajectories is the final result of this iteration.

B. DETECTING THE TRACKLETS BY 3DHT

The parameter space discretization is the most fundamental constituent of this Hough Transform. A 3-dimensional accumulator array with each cell representing one set of three parameters from the discretized parameter space is built in

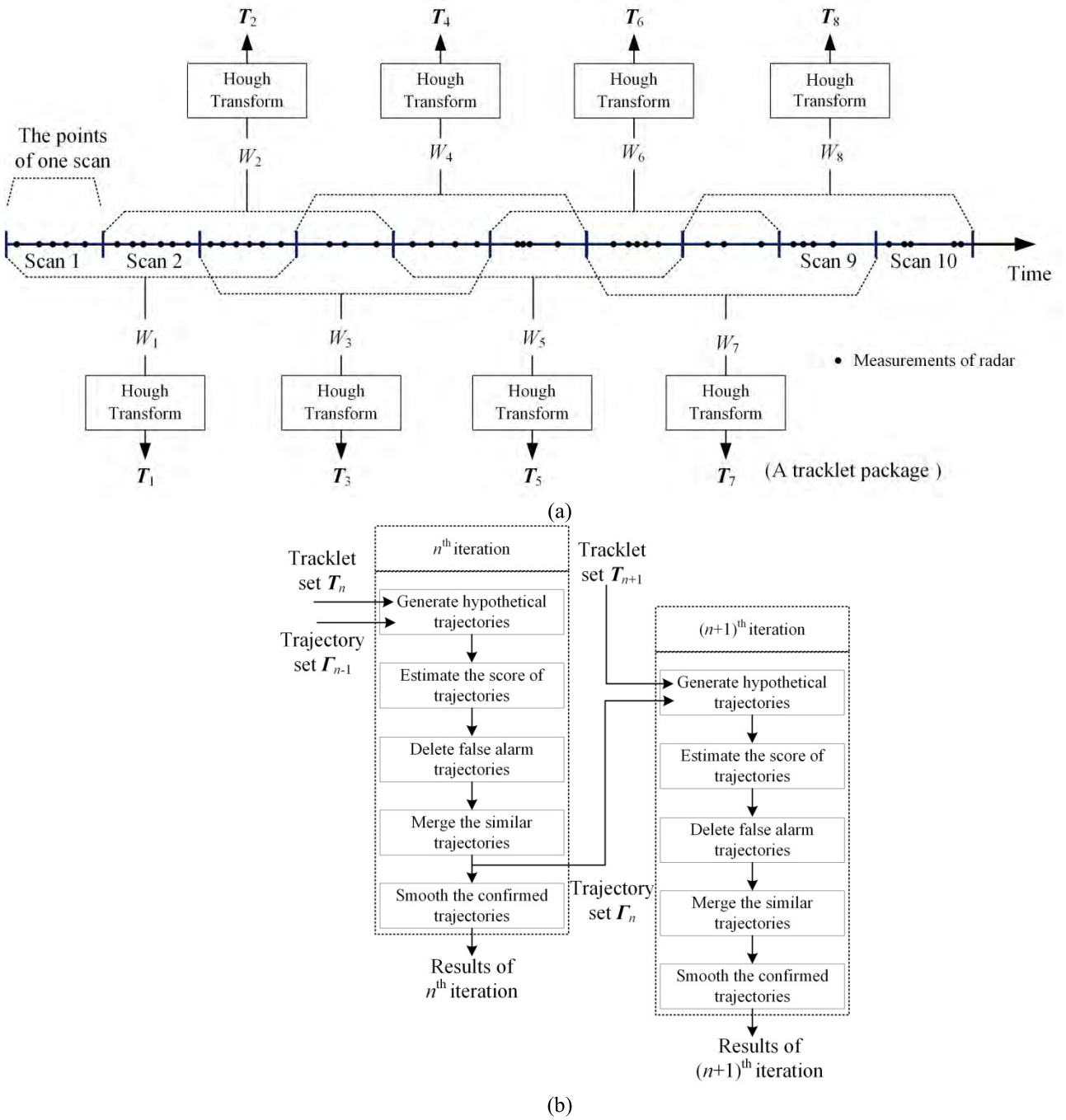

FIGURE 2. (a) The schematic diagram of 3DHT. (b) The iteration of the track-to-track MHT.

the 3DHT. Each set of three parameters corresponding to a straight line in 3D. The position of the 3D-line at the horizontal plane, Time equals 0, is represented by an anchor point. The horizontal plane can be divided into $N_x \times N_y$ grid cells and the two parameters are utilized to indicate the arbitrary grid cell. The direction of the line corresponding to the is the third parameter. As is presented in figure 3a.

However, not all the direction vectors are suitable to indicate the direction of a tracklet. In this work, the line direction is corresponding to the kinematic state of the target. θ represents the course of the target in 2D coordinate plane and ϕ means the velocity. The specific relationship of the variates can be concluded by (11)

$$\begin{cases} a = \dfrac{e_y}{e_x} = \tan(\theta) \\ v = \dfrac{\sqrt{e_x^2 + e_y^2}}{e_t} = \arctan(\phi) \end{cases} \tag{7}$$

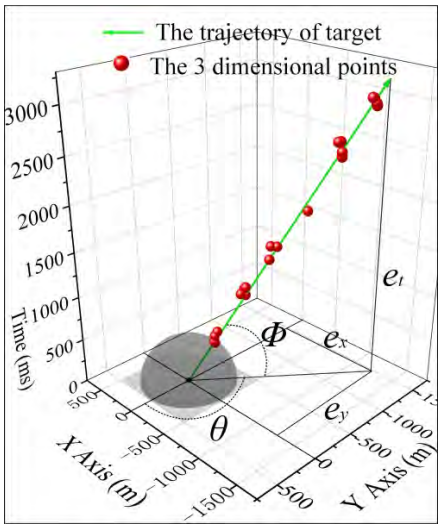

(a)

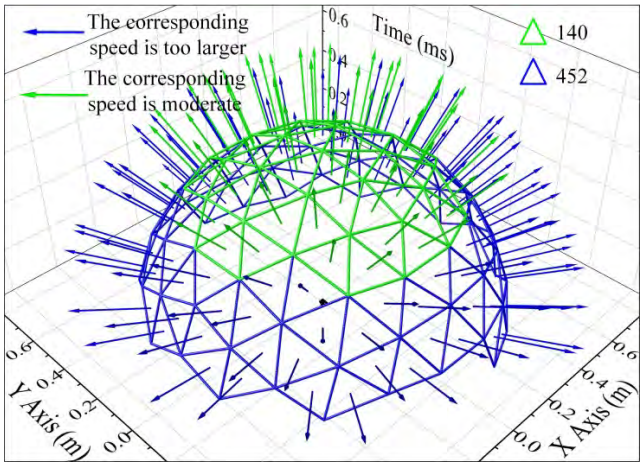

(b)

FIGURE 3. (a) The points and tracklet of an extended target. (b) The candidate direction of 3D-lines.

For the limitation of the target velocity, ϕ should meet the following criterion:

$$\begin{cases} \arctan(\phi) \le v_{\max} \\ 0 \le \phi \le \dfrac{\pi}{2} \end{cases} \tag{8}$$

The $v_{\max}$ is the maximum velocity of targets and it is set as 1000m/s. The appropriate directions are presented by the green vectors in figure3b. Meanwhile, the direction vectors whose corresponding velocity larger than the up limit $v_{\max}$ are indicated by the vectors and triangles in blue. The appropriate direction vectors are devoted to its application for making a list where each appropriate direction vector is assigned a number. Then, the direction of the line can be indicated by one parameter, i.e. the sequence number of the direction in the list. The quantity of the direction vectors is represented by N_d, the N_d equals 140 in this work. Since three parameters are enough to indicate a 3D-line, the parameter space of the HT has 3 dimensions, i.e. the parameter space is an accumulator array which has $N_x \times N_y \times N_d$ grid cells.

The next step is to transform the measurements into the parameter space. Each measurement votes N_d times for the accumulator array, i.e. each direction vector has a vote. A location (x',y') can be obtained given the measurement (x_i, y_i, t_i) and a direction vector (e_x, e_y, e_t) illustrated in Eq.(9). The (x',y') is defined as the coordinates of the intersection of the line and the plane in the plane's own 2D coordinate frame of the plane.

$$\begin{cases} x' = (1 - \dfrac{e_x^2}{1+e_t})x_i - (\dfrac{e_x e_y}{1+e_t})y_i - e_x t_i \\ y' = -(\dfrac{e_x e_y}{1+e_t})x_i + (1 - \dfrac{e_y^2}{1+e_t})y_i - e_y t_i \end{cases} \tag{9}$$

It assumes that the sequence number of the direction vector (e_x, e_y, e_t) is n_d. The cell (n_x, n_y, n_d) which would be voted by the measurement (x_i, y_i, t_i) can be obtained by:

$$\begin{pmatrix} e_x \\ e_y \\ e_t \end{pmatrix} = \begin{pmatrix} \cos\theta\cos\phi \\ \sin\theta\cos\phi \\ \sin\phi \end{pmatrix} \tag{10}$$

$$\begin{cases} n_x = \left\lfloor (x' + \dfrac{d_{\max}}{2}) \dfrac{d_{\max}}{N_x - 1} \right\rfloor \\ n_y = \left\lfloor (y' + \dfrac{d_{\max}}{2}) \dfrac{d_{\max}}{N_y - 1} \right\rfloor \end{cases} \tag{11}$$

Parameter $d_{\max}$ in equation (12) indicates the maximum distance between the original point and the measurements.

$$d_{\max} = \max(\sqrt{(x_k^i)^2 + (y_k^i)^2 + (t_k^i)^2}), \quad i = 1, \ldots, N_k \tag{12}$$

After introducing the parameter space discretization, the iteration of the 3DHT is showcased. In the iteration, we only looking for the highest voted cell. Then, backtrace the 3D-line corresponding to the highest voted cell. The measurements belonging to the 3D-line are then identified and removed from the points in the window. Then, the Hough transform is applied again to the remaining measurements for finding next tracklet. The iteration stops when all the tracklets have been detected. The iteration consists of several following steps.

Step 1, the parameter space for all the lines crossing the points are discrete to build the accumulator array which has $N_x \times N_y \times N_d$ voting cells.

Step 2, the 3D Hough Transform of the points are performed. The votes of the points to the voting cells can be calculated by Eq.(9-11).

Step 3, the line parameters corresponding to the highest voted accumulator cell is exploited to find the most appropriate tracklet. The tracklet can be represented by an anchor point $\boldsymbol{a}_1$ and a 3-dimensional direction vector $\boldsymbol{b}_1$. The anchor point $\boldsymbol{a}_1$ can be calculated by equation (13) when the highest voted accumulator cell is (n_x, n_y, n_d). The vector $\boldsymbol{b}_1$ can be

obtained by the number of the vector n_d and the direction vector list.

$$\begin{cases} x' = n_{xo}\dfrac{n_x - 1}{d_{\max}} \\ y' = n_{yo}\dfrac{n_y - 1}{d_{\max}} \end{cases} \tag{13}$$

Step 4, all the measurements close to the candidate tracklet would be found in this step. The criterion for determining whether a measurement $\boldsymbol{z}$ belongs to a tracklet given in the form of the vector $\boldsymbol{a}_1 + \boldsymbol{b}_1$ is that its perpendicular distance to the tracklet d is less than a fixed width threshold T_d.

$$T_d < d, d = \|z - (\boldsymbol{a}_1 + \langle \boldsymbol{b}_1, z - \boldsymbol{a}_1 \rangle \boldsymbol{b}_1)\| \tag{14}$$

The set of the adjacent points is represented by a parameter $\boldsymbol{Y}$.

$$z = \begin{bmatrix} x_i \\ y_i \\ t_i \end{bmatrix}, \quad \boldsymbol{a}_1 = \begin{bmatrix} x' \\ y' \\ 0 \end{bmatrix}, \ \boldsymbol{b}_1 = \begin{bmatrix} e_x \\ e_y \\ e_t \end{bmatrix} \tag{15}$$

Step 5, a more accurate straight line can be obtained by the adjacent points in set $\boldsymbol{Y}$ with an orthogonal least squares fit. The anchor point $\boldsymbol{a}_2$ and the direction vector $\boldsymbol{b}_2$ of the optimal line can be obtained by Eq.(17-18).

$$\boldsymbol{a}_2 = \begin{bmatrix} \sum_{i=1}^{|\boldsymbol{Y}|} x_i \Big/ |\boldsymbol{Y}| \\ \sum_{i=1}^{|\boldsymbol{Y}|} y_i \Big/ |\boldsymbol{Y}| \\ \sum_{i=1}^{|\boldsymbol{Y}|} t_i \Big/ |\boldsymbol{Y}| \end{bmatrix} = \begin{bmatrix} x_a \\ y_a \\ t_a \end{bmatrix} \tag{16}$$

$$\boldsymbol{Q} = \boldsymbol{q}\boldsymbol{q}^{\mathrm{T}}; \boldsymbol{q} = \begin{bmatrix} (x_1 - x_a) & \cdot & (x_{|\boldsymbol{Y}|} - x_a) \\ (y_1 - y_a) & \cdot & (y_{|\boldsymbol{Y}|} - y_a) \\ (t_1 - t_a) & \cdot & (t_{|\boldsymbol{Y}|} - t_a) \end{bmatrix} \tag{17}$$

$$\boldsymbol{Q}\begin{bmatrix} e_x \\ e_y \\ e_t \end{bmatrix} = \begin{bmatrix} e_x \\ e_y \\ e_t \end{bmatrix}\lambda, \quad \boldsymbol{b}_2 = \begin{bmatrix} e_x \\ e_y \\ e_t \end{bmatrix} \tag{18}$$

Step 6, similar with the step 4, all points from $\boldsymbol{Z}$ close to the optimal line can be selected by Eq.(19). The adjacent points are stored in set $\boldsymbol{Y}$.

$$T_d < d, \quad d = \|z - (\boldsymbol{a}_2 + \langle \boldsymbol{b}_2, z - \boldsymbol{a}_2 \rangle \boldsymbol{b}_2)\| \tag{19}$$

Step 7, the iteration would be terminated if $\boldsymbol{Y}$ contains too few points. Otherwise, a tracklet in this widow is confirmed. The set $\boldsymbol{Y}$ would be stored in the tracklet set $\boldsymbol{T}$. The points of $\boldsymbol{Y}$ are removed from the set $\boldsymbol{Z}$. The votes casted by the points of $\boldsymbol{Y}$ should be subtracted from the accumulator array. Then, turn to the step 3 for next tracklet until all the tracklets are found out.

For a better description, the pseudocode of the 3DHT is showcased in table 1. The more accurate introduction of the 3DHT is available in our former work [9].

TABLE 1. The pseudocode of the 3DHT.

Input: 3-dimensional points in a window
$\boldsymbol{Z}=\{(x_i, y_i, t_i)|i=1,\ldots,N\}$
Output: The tracklets in this window $\boldsymbol{T}$
For i=1:N
  For j=1:N_d
    (x', y′)←Computed after Eq.(9).
    (n_x, n_y)←Computed after Eq.(11).
    $\boldsymbol{A}(n_x, n_y, j)$←$\boldsymbol{A}(n_x, n_y, j)$+1
Repeat
  (n_{xo}, n_{yo}, n_{to})←Cell corresponding to maximum of $\boldsymbol{A}$
  $\boldsymbol{Y}$←{ }
  For each (x_i, y_i, t_i) in $\boldsymbol{Z}$
    IF Eq.(14-15) holds
      $\boldsymbol{Y}$←$\boldsymbol{Y}\bigcup(x_i, y_i, t_i)$
      (x,y,t) ←orthogonal least squares fitted line to $\boldsymbol{Y}$
  $\boldsymbol{Y}$←{ }
  For each (x_i, y_i, t_i) in $\boldsymbol{Z}$
    If Eq.(16) holds
      $\boldsymbol{Y}\leftarrow\boldsymbol{Y}\bigcup(x_i, y_i, t_i)$
  IF |Y|<$n_{\min}$
    Break (End of the 3DHT)
  Else
    Remove the points in $\boldsymbol{Y}$ from $\boldsymbol{Z}$
    For each (x_i, y_i, t_i) in $\boldsymbol{Y}$
      For j=1:N_d
        (x', y′)←Computed after Eq.(9).
        (n_x, n_y)←Computed after Eq.(11).
        $\boldsymbol{A}(n_x, n_y, j)$←$\boldsymbol{A}(n_x, n_y, j)$-1
    $\boldsymbol{T}\leftarrow\boldsymbol{T}\bigcup$ Y

C. ASSOCIATING THE TRACKLETS BY MHT

The MHT aims to find the optimal global hypothesis and the particular hypotheses is used for track maintenance. The global hypothesis is a set of trajectories that are compatible, that is not in conflict: any two trajectories in a global hypothesis do not share any tracklets [25].

The input of the MHT is the maintained trajectories $\boldsymbol{\Gamma}_n$ and the tracklets obtained in n^{th} window $\boldsymbol{T}_n$. It assumes that M trajectories and N tracklets exist in the set of $\boldsymbol{\Gamma}_n$ and $\boldsymbol{T}_n$ respectively, i.e.

$$\begin{cases} \boldsymbol{T}_n = \{\boldsymbol{T}_n^1, \ldots, \boldsymbol{T}_n^N\} \\ \boldsymbol{\Gamma}_n = \{\boldsymbol{\Gamma}_n^1, \ldots, \boldsymbol{\Gamma}_n^M\} \end{cases} \tag{20}$$

The first step in this stage is finding the optimal track-to-track associations. The distance between each pair of trajectory and tracklet would be calculated before the association. The distance between Γ_n^i and $\boldsymbol{T}_n^j$ can be represented by d_{ij}. The points of the Γ_n^i in the window n are compared with the points in $\boldsymbol{T}_n^j$. The sets of the points in Γ_n^i and $\boldsymbol{T}_n^j$ are

represented by $\boldsymbol{P}$ and $\boldsymbol{Q}$ respectively.

$$\begin{aligned}\boldsymbol{P} &= \{\boldsymbol{P}_a \,|a = 1, \ldots, |\boldsymbol{P}|\}; \boldsymbol{P_a} = (x_a, y_a, t_a)\\ \boldsymbol{Q} &= \{\boldsymbol{Q}_b \,|b = 1, \ldots, |\boldsymbol{Q}|\}; \boldsymbol{Q}_b = (x'_b, y'_b, t'_b)\end{aligned} \tag{21}$$

$$d_{ij} = \begin{cases} D(\boldsymbol{P}, \boldsymbol{Q}), |\boldsymbol{P}| > |\boldsymbol{Q}| \\ D(\boldsymbol{Q}, \boldsymbol{P}), |\boldsymbol{P}| \leq |\boldsymbol{Q}| \end{cases} \tag{22}$$

$$\begin{aligned}D(\boldsymbol{P}, \boldsymbol{Q}) = &(\frac{1}{|\boldsymbol{P}|} (\min_{\kappa \in \Omega}) \sum_{i=1}^{|\boldsymbol{Q}|} (d(\boldsymbol{Q}_i, \boldsymbol{P}_{\kappa(i)}))^p \\ &+ (|\boldsymbol{P}| - |\boldsymbol{Q}|)c^p))^{1/p}, |\boldsymbol{P}| > |\boldsymbol{Q}|\end{aligned} \tag{23}$$

$$d(\boldsymbol{Q}_a, \boldsymbol{P}_b) = \sqrt{(x_a - x'_b)^2 + (y_a - y'_b)^2 + (t_a - t'_b)^2} \tag{24}$$

Ω represents the set of permutations of length $|\boldsymbol{Q}|$ with elements taken from $\boldsymbol{P}$. The parameter c and p represent the cut-off value and the distance order. Note that the cut-off parameter c determines the relative weighting given to the cardinality error component against the localization error component. Smaller values of c tend to emphasize localization errors and vice versa. Then, a distance array can be obtained.

$$\boldsymbol{D} = \begin{bmatrix} d_{11} & d_{12} & \ldots & d_{1N} \\ \vdots & \vdots & \ddots & \vdots \\ d_{M1} & d_{M2} & \ldots & d_{MN} \end{bmatrix} \tag{25}$$

Exhaustively list all possible trajectory-to-tracklet associations infeasible for the computation. The distance array is performed to remove the most unlikely tracklets of each trajectory. Only those tracklets whose distance is less than a fixed distance threshold are considered for the association of the trajectory.

Clustering is performed with the utilization of the distance array $\boldsymbol{D}$ to break the large association problem into small sub-problems. The clustering process partitions the full set of track hypotheses into a number of disjoint groups and thus the trajectory-to-tracklet association can be done in a parallel way to improve the computational efficiency. A smaller fixed distance threshold means that the set of track hypotheses can be partitioned into more disjoint groups. Fewer hypotheses would exist in one group. Now, all possible trajectory-to-tracklet associations of each group can be listed. The optimal global trajectory-to-tracklet associations in each group can be obtained. The points of the tracklets and its corresponding trajectory are merged as an updated trajectory.

$$\boldsymbol{P} \leftarrow \boldsymbol{P} \cup \boldsymbol{Q} \tag{26}$$

New trajectories are constructed for each unassociated tracklet to consider the possibility the new tracklet being a new target. Unassociated trajectories are still reserved in the trajectory set.

The second step is to estimate the score of trajectories in the set. Each trajectory is associated with a track score, which is typically defined as a log likelihood ratio between the true target hypothesis probability and false alarm hypothesis probability. The true target hypothesis assumes that the points come from the same target whereas the false alarm hypothesis assumes the points originates from clutter. A track is immediately deleted if its score is below the lower threshold.

The scores of each trajectory can be estimated in three aspects, i.e. the kinematic state, the measurement rate and the extension of the target. It assumes that N points exist in a set representing a trajectory.

$$\boldsymbol{\Gamma}^i = \{\boldsymbol{z}^j | j = 1, \ldots, N\} = \{(x^j, y^j, t^j) | j = 1, \ldots, N\} \tag{27}$$

The three functions $F_\gamma(\bullet)$, $F_{\boldsymbol{x}}(\bullet)$ and $F_{\boldsymbol{X}}(\bullet)$ represent the probability that the set $\Gamma^i$is generated by the target using the information of measurement rate, target position, target extension respectively.

$$F(\Gamma^i) = F_{\mathrm{x}}(\boldsymbol{\Gamma}^i) F_\gamma(\boldsymbol{\Gamma}^i) F_{\mathrm{X}}(\boldsymbol{\Gamma}^i) \tag{28}$$

An estimated location $(\dot{x}^a, \dot{y}^a)$ can be obtained by the other points in this track $\{\boldsymbol{z}^j | j = 1, \ldots, N; j \neq a\}$.

$$(\dot{x}^a, \dot{y}^a) = F(t^a, \boldsymbol{z}^j | j = 1, \ldots, N; j \neq a) \tag{29}$$

Then the $F_{\mathrm{x}}(\boldsymbol{z}^j)$ in Eq.(30) can be estimated by

$$\begin{aligned}F_{\mathrm{x}}(\boldsymbol{z}^j) &= \frac{1}{\sqrt{2\pi}\sigma} \exp(-\frac{d}{2\sigma^2});\\ d &= \sqrt{(\dot{x}^a - x^a)^2 + (\dot{y}^a - y^a)^2}\end{aligned} \tag{30}$$

$$F_{\mathrm{x}}(\boldsymbol{\Gamma}^i) = \sum_{j=1}^{N} \log(F_{\mathrm{x}}(\boldsymbol{z}^j)) \tag{31}$$

Meanwhile, the points are partitioned into clusters by the scans, each cluster is the set of points originated from the same target in one scan.

$$\begin{aligned}\boldsymbol{\Gamma}^i &= \{\{z\}_t^i | t = k_{\mathrm{s}}, \ldots, k_{\mathrm{e}}\};\\ \{z\}_t^i &= \{(x_t^j, y_t^j, t_t^j) | j = 1, \ldots, |\{z\}_t^i|\}\end{aligned} \tag{32}$$

$\{z\}_t^i$ represents the points generated by the i^{th} target at k^{th} scan. The measurement rate γ of extended targets is assumed invariant during the scans. The measurement rate γ approximate to the average number of the measurements in these sets.

$$\gamma = \frac{\sum_{t=k_{\mathrm{s}}}^{k_{\mathrm{e}}} \left|\{z\}_t^i\right|}{k_{\mathrm{e}} - k_{\mathrm{s}} + 1} \tag{33}$$

Then the $F_\gamma(\{z\}_t^i)$ can be estimated by

$$F_{\boldsymbol{\gamma}}(\{z\}_t^i) = \frac{\gamma^{|\{z\}_t^i|}}{|\{z\}_t^i|!} \exp(-\gamma) \tag{34}$$

$$F_\gamma(\Gamma^i) = \sum_{t=k_{\mathrm{s}}}^{k_{\mathrm{e}}} \log(F_\gamma(\{z\}_t^i)) \tag{35}$$

As to the target extension $F_{\boldsymbol{X}}(\{z\}_t^i)$, extension state $\boldsymbol{X}_k$ is described an inverse Wishart probability distribution function (PDF). $\boldsymbol{IW}_d(\boldsymbol{X}; v, V)$ in Eq.(35) denotes an inverse Wishart pdf defined over the matrix $\boldsymbol{X}$ with degrees of

freedom v and parameter matrix V[26, pp.111].

$$F_X(\{z\}_t^i) = \boldsymbol{IW}_d(\boldsymbol{X}_t^i; v^i, V^i) = \frac{2^{-\frac{v^i-d_X-1}{2}}|V^i|^{-\frac{v^i-d_X-1}{2}}}{\Gamma_{d_X}(\frac{v^i-d_X-1}{2})|\boldsymbol{X}_k^i|^{\frac{v^i}{2}}}\exp(Tr(-\frac{1}{2}(\boldsymbol{X}_k^i)^{-1}V^i)) \tag{36}$$

where $\Gamma_d(\bullet)$ is the multivariate gamma function, $d_{\boldsymbol{X}}$ means the dimension of the matrix $\boldsymbol{X}$ and Tr($\bullet$) denotes the trace of a matrix. Degrees of freedom v and parameter matrix V can be estimated by the measurement sets $\{\{z\}_t^i | t = k_s, \ldots, k_e\}$ by equation (37) and equation (38)

$$v^i = \frac{\sum_{t=k_s}^{k_e}|\{z\}_t^i|}{k_e - k_s + 1} \tag{37}$$

$$V^i = \frac{\sum_{t=k_s}^{k_e}\overline{\boldsymbol{Z}}_t^i}{k_e - k_s + 1} \tag{38}$$

The $\overline{\boldsymbol{Z}}_t^i$ denote the scatter matrix of the set $\{z\}_t^i$.

$$\overline{\boldsymbol{Z}}_t^i = \sum_{z\in\{z\}_t^i}(z - \overline{z}_t^i)(z - \overline{z}_t^i)^{\mathrm{T}} \tag{39}$$

The $\overline{z}_t^i$ is the centroid measurement of the set.

$$\overline{z}_t^i = \frac{\sum_{z\in\{z\}_t^i} z}{|\{z\}_t^i|} \tag{40}$$

The extension state of the i^{th} target in scan t can be estimated by Eq.(41)

$$\boldsymbol{X}_t^i = \frac{\overline{\boldsymbol{Z}}_t^i}{|\{z\}_t^i| - 2d - 2} \tag{41}$$

Then, the extension state of the trajectory can be estimated by Eq.(42)

$$F_X(\boldsymbol{\Gamma}^i) = \sum_{t=t_s}^{t_e}\log(F_X(\{z\}_t^i)) \tag{42}$$

A track is immediately deleted if its target likelihood ratio $F(\Gamma^i)$ is below the lower threshold.

$$\begin{cases} F(\boldsymbol{\Gamma}^i) \geq P_{\min}; & \text{Reserved trajectory} \\ F(\boldsymbol{\Gamma}^i) < P_{\min}; & \text{False alarm trajectory} \end{cases} \tag{43}$$

The reserved trajectories in the set would be further tested in the next iteration, i.e. the set of updated trajectories $\boldsymbol{\Gamma}_{n+1}$.

The third step is to merge the similar trajectories. Two trajectories which share quite a few points should be merged as one trajectory. It assumes that the trajectory set in this step is $\boldsymbol{\Gamma}_n = \{\boldsymbol{\Gamma}_n^1, \ldots, \boldsymbol{\Gamma}_n^M\}$. The distance between the two elements $\boldsymbol{\Gamma}_n^i$ and $\boldsymbol{\Gamma}_n^j$ can be calculated by

$$d_{ij} = \begin{cases} D(\boldsymbol{\Gamma}_n^i, \boldsymbol{\Gamma}_n^j), |\boldsymbol{\Gamma}_n^i| > \left|\boldsymbol{\Gamma}_n^j\right| \\ D(\boldsymbol{\Gamma}_n^j, \boldsymbol{\Gamma}_n^i), |\boldsymbol{\Gamma}_n^i| \leq \left|\boldsymbol{\Gamma}_n^j\right| \end{cases} \tag{44}$$

$$D(\boldsymbol{\Gamma}_n^i, \boldsymbol{\Gamma}_n^j) = (\frac{1}{|\boldsymbol{\Gamma}_n^i|}(\min_{\kappa\in\Omega}\sum_{t=1}^{\left|\boldsymbol{\Gamma}_n^j\right|}(d(\boldsymbol{\Gamma}_n^{j,t}, \boldsymbol{\Gamma}_n^{i,\kappa(i)})^p + (\left|\boldsymbol{\Gamma}_n^i\right| - \left|\boldsymbol{\Gamma}_n^j\right|)c^p))^{1/p}, \quad \left|\boldsymbol{\Gamma}_n^i\right| > \left|\boldsymbol{\Gamma}_n^j\right| \tag{45}$$

The two trajectories $\boldsymbol{\Gamma}_n^i$ and $\boldsymbol{\Gamma}_n^j$ would be merged if the distance d_{ij} less than a fixed threshold. After merging the similar tracks, the trajectories whose score exceeds the upper threshold are regarded as the confirmed trajectories.

$$\begin{cases} F(\boldsymbol{\Gamma}^i) \geq P_{\text{con}}; & \text{Confirmed trajectory} \\ F(\boldsymbol{\Gamma}^i) < P_{\text{con}}; & \text{Candidate trajectory} \end{cases} \tag{46}$$

The confirmed trajectories are represented by a series of points. The fourth step is still necessary to smooth the confirmed trajectories [27], [28]. An orthogonal least squares fitting can be applied on each confirmed trajectory for a more accurate trajectory for efficiency. The steps of the orthogonal least squares fitting can be acquired in our former work [9].

The diagram of utilizing the 3DHT-MHT in a real scenario is presented in figure 4. The measurements are presented by the blue points in figure 4a. The source of the points is unknown. In figure 4b, the tracklets obtained by the 3DHT in different windows are represented by the vectors in different colors. Vectors in blue and red denote the tracklets in the first and the last window. The false alarm tracklets are randomly distributed in the 3-dimensional space. The false tracklets are hard to associate with the others. Therefore, very few false alarm trajectories would be built in the 3DHT-MHT. The red points in figure 4c denote the points originated from a maneuvering extended target. The continuous line inside these points represents the smoothed trajectory after the orthogonal least squares fitting. Figure 4 showcases the ability of 3DHT-MHT in maneuvering extended target detection and tracking.

D. COMPLEXITY OF THE 3DHT-MHT

In this section, the computation complexity of the 3DHT-TBD is evaluated. The run-time of the target tracking algorithms begins when the point set $\boldsymbol{Z}^k$ is fed to the program and ends when the trajectory of each target is obtained. Computation of the 3DHT-MHT is mainly consists of three parts. The first is the computation of the Hough transformation. Eq.(9) and Eq.(11) are repeatedly applied $|\boldsymbol{Z}^k| \times N_d$ times. It assumes that calculating Eq.(9) and Eq.(11) costs about 30 mathematical operations. Then, the calculation of this part equals $30\times|\boldsymbol{Z}^k| \times N_d$. The second is the computation of finding the current optimal tracklet, it is related to the number of cells $N_x \times N_y \times N_d$ and the quantity of obtained tracklets $|\boldsymbol{T}_k|$. The calculation can be approximate by $N_x \times N_y \times N_d \times |\boldsymbol{T}_k|$. The third is the computation of tracklets association. It is related to the number of tracklets $|\boldsymbol{T}_k|$ and the number of the candidate trajectories $|\Gamma_k|$. The computation of the 3DHT-MHT can be expressed by Eq.(47) if evaluating one pair of association costs m mathematical operations.

$$30\,N_d \times |\boldsymbol{Z}^k| + N_x N_y N_d |\boldsymbol{T}_k| + m \times |\boldsymbol{T}_k| \times |\Gamma_k| \tag{47}$$

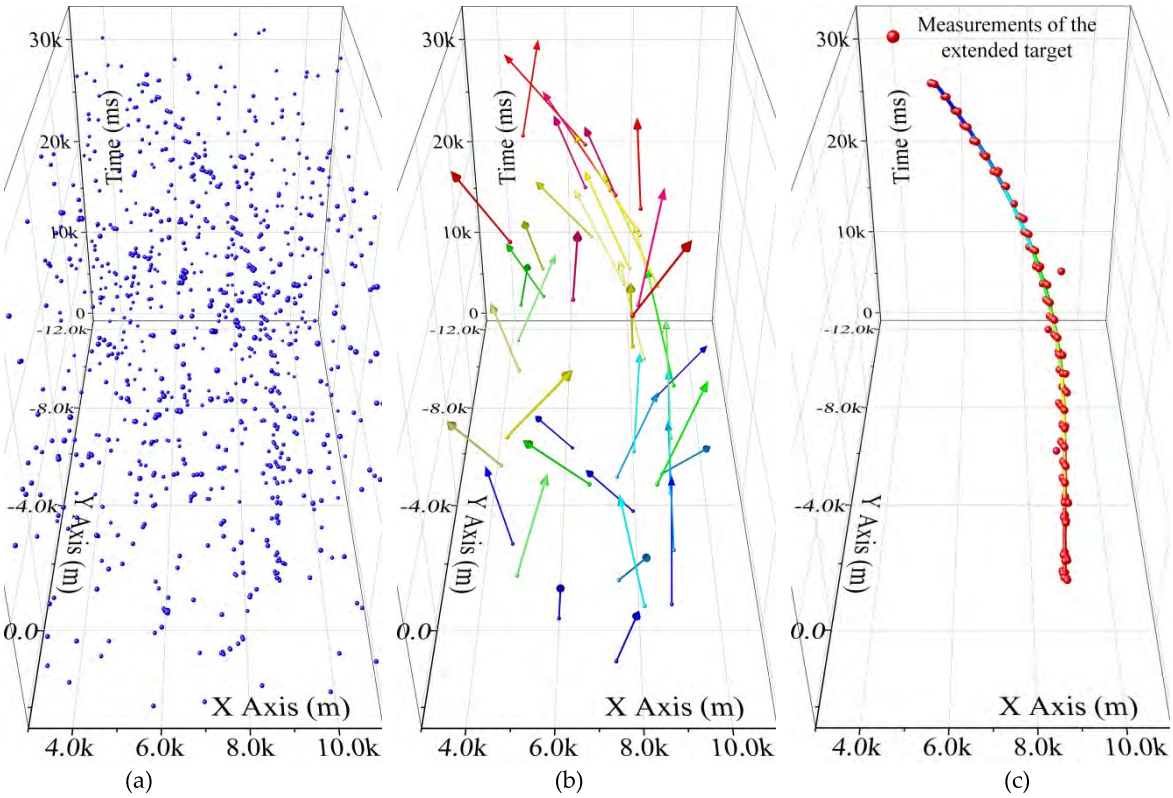

FIGURE 4. The utilization of the 3DHT-MHT in a real scenario. (a) The measurements of the radar. (b) The tracklets obtained by the 3DHT in different time windows. (c) The smoothed trajectory and its measurements.

The computation of 3DHT-TBD consists of two parts, i.e. the first two elements in Eq.(47). Therefore, the 3DHT-MHT would take $m \times |\boldsymbol{T}_k| \times |\Gamma_k|$ more mathematical operations. However, the $m \times |\boldsymbol{T}_k| \times |\Gamma_k|$ is much smaller than the first two elements in Eq.(47) because both the quantity of tracklets and the quantity of trajectories are far less than that of points. Meanwhile, for the utilization of tracklets clustering by Eq.(25). The realistic computation of tracklets association is far less than $m \times |\boldsymbol{T}_k| \times |\Gamma_k|$. Therefore, the computation of the 3DHT-MHT is slightly larger than that of 3DHT-TBD. Meanwhile, the computation of the 3DHT-MHT and other mentioned approaches would be evaluated and compared in the following section.

IV. SIMULATION RESULTS

A. SYNTHETIC DATA

In this section, extensive experiments are conducted to verify the feasibility of the proposed model from different aspects including robustness against various scenes, robustness to measurement noise, the ability of background suppression and target enhancement, target detection ability, and the computation time of the algorithm. To fully access the superiority of the proposed algorithm, three state-of-the-art approaches are also performed for comparison. Both the PHD filter based approaches and track-before-detect methods are compared with the 3DHT-MHT. In the category of PHD approaches, the distance partition method [3], the ART partition method [6] are combined with the PHD [3] respectively. In the category of TBD approaches, the 3DHT-TBD [9] is performed. The 200 Monte Carlo numerical simulations are performed on the Intel Core I7-4790, 3.6GHz with 4GB RAM in Matlab R2016a environment.

Figure 5a shows the scenario of 8 turning tracks. They began circular motion at 11 seconds and moved uniformly again from 26 to 30 seconds. In this work, 8 scenarios are considered, the measurement noise and the false alarm rate are various in each scenario. The detailed parameters of the scenarios are presented in Table 2. The scenarios 1,2 and 3 are different in measurement noise. The scenarios 2, 4 and 5 are used to explore the impact of false alarm. The compared between the scenarios 1, 4, 5 and the scenarios 6, 7, 8 are different in measurement rate. The targets in scenarios 6, 7, 8 are weak targets.

Figure 6b, shows the synthetic data in scenarios 1, 2, 5 and 8. Naked eyes are difficult to detect the targets in these scenarios. The points in red and blue represent the points originated from targets and clutter respectively. However, the points are unlabeled in processing. The targets are hard to be followed by naked eyes, especially in scenario 8.

The optimal sub-pattern assignment (OSPA) distance [29] are used for evaluating the performance of the algorithms. The cut-off value and the distance order of OSPA distance are set as 500 and 1 in this work. The cut-off parameter determines the relative weighting given to the cardinality

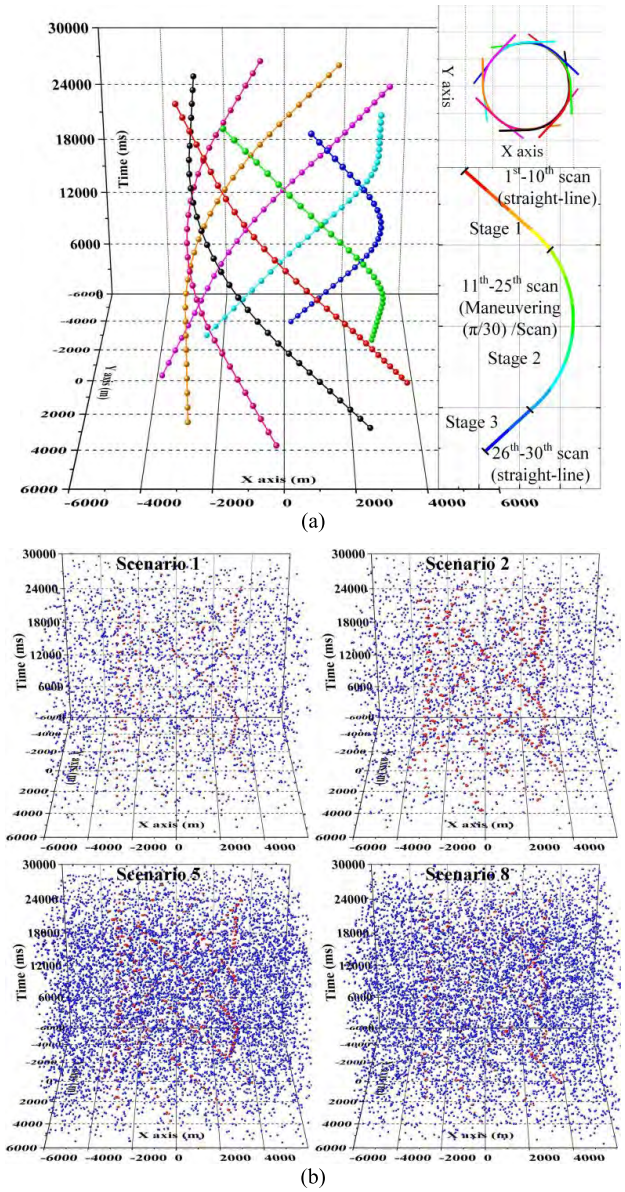

FIGURE 5. **(a) The trajectory of the simulated targets. (b) The synthetic measurements.**

error component against the localization error component. The results of the four algorithms at each scan are presented in figure 6. Figure 6a corresponds to scenario 1, and so on. A smaller OSPA distance means a better tracking performance.

At stage 1, 1st-10th scans, the performance of the 3DHT-MHT is similar with the two PHD filter based methods in general and being the best in scenarios 1, 2, 7 and 8. The PHD filter works well in stage 1 is mainly because the initial state of the extended targets is given. The 3DHT is intentionally designed for straight line detection. The 3DHT-TBD is worse than the others in scenarios 5 and 8 because lots of false trajectories are built for the dense clutter.

In stage 2, the targets are maneuvering and the performance of the methods is deteriorated. However, it is obvious that the effect of the targets maneuvering is different. The performance of the 3DHT-MHT is better than the others. The 3DHT-TBD is designed for straight line detection, the method is greatly deteriorated for the low detection rate in this stage. In some severe scenarios, such as scenarios 4 and 5, the PHD filter is hard to maintain the detected trajectories. The distance partition method is worse than the ART based partition method mainly because the distance partition method generates more incorrect partitions.

The OSPA distance of the stage 3 is smaller than the stage 2 but larger than the stage 1 in general mainly because that the targets have been lost in stage 2 but detecting a normal target is easier than detecting a maneuvering target. The 3DHT-MHT is always better than the others because the trajectories are not lost in stage 2. Maintaining the straight trajectories in stage 3 by 3DHT-MHT is much easier than detect the targets again in the other 3 methods.

In general, the 3DHT-MHT is no worse than the others in stage 1 and is obviously superior to the others in stage 2 and 3. The average OSPA distance of the four methods is patched in Table 3. It infers that the 3DHT-MHT outperforms the others in all 8 scenarios.

The cardinality error component in OSPA distance includes two aspects, target detection rate and the number of false trajectories. The average detection rate and the average false alarm number of the 8 scenarios are patched in table 4 to further analyze the superiority of the proposed method.

In scenarios 1-5, the average detection rate of normal targets with the 3DMT-MHT is always higher than the others. The false alarm number of the 3DHT-MHT and 3DHT-TBD is proportional to the number of false alarm points. The false

TABLE 2. **The parameters of the scenarios.**

	Measurement rate γ	Measurement noise (m)	Number of clutter per squre ($1/m^2$)
Scenario 1	4	10	6×10^{-7}
Scenario 2	4	50	6×10^{-7}
Scenario 3	4	100	6×10^{-7}
Scenario 4	4	50	1.2×10^{-6}
Scenario 5	4	50	1.8×10^{-6}
Scenario 6	2	10	6×10^{-7}
Scenario 7	2	50	1.2×10^{-6}
Scenario 8	2	50	1.8×10^{-6}

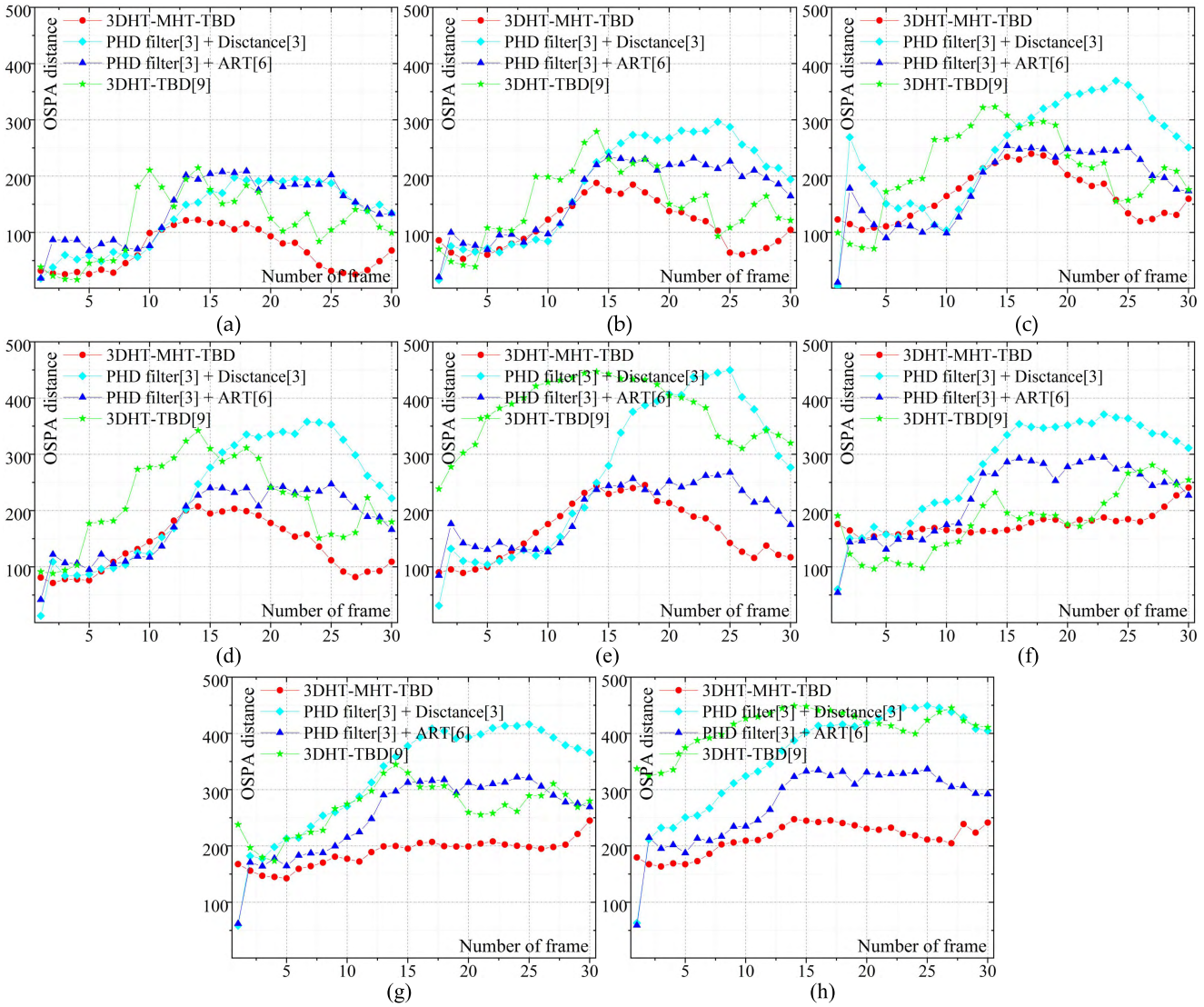

FIGURE 6. The OSPA distance of the four approaches.

TABLE 3. Average OSPA distance of the methods.

	3DHT-MHT	PHD [3]+ Distance [3]	PHD [3]+ ART[6]	3DHT-TBD [9]
Scenario 1	67.52	129.54	141.78	118.19
Scenario 2	112.32	183.63	164.21	152.93
Scenario 3	165.48	245.19	182.5	214.7
Scenario 4	136.44	223.06	178.56	217.99
Scenario 5	165.32	265.29	196.53	377.46
Scenario 6	177.2	276.06	222.84	183.07
Scenario 7	188.39	323.44	254.31	268.12
Scenario 8	213.63	356.21	274.46	409.43

alarm number of 3DHT-MHT is similar with those of the PHD filters and much less than that of the 3DHT-TBD. As to the weak targets, i.e. scenarios 6-8, the detection rate of the methods is similar. However, far less false alarm trajectories are built by the 3DHT-MHT. In summary, the 3DHT-MHT has a higher detection rate in detecting normal targets and has built less false trajectories in detecting weak targets.

TABLE 4. Results of the methods.

	Average detection rate of 8 targets				Average false alarm number			
	3DHT-MHT	PHD [3]+ Distance [3]	PHD [3]+ ART [6]	3DHT-TBD [9]	3DHT -MHT	PHD [3]+ Distance [3]	PHD [3]+ ART [6]	3DHT-TBD [9]
Scenario 1	98.97	91.25	95.73	96.28	1.116	0.994	1.308	2.237
Scenario 2	98.81	94.22	96.28	97.07	1.701	1.882	1.973	2.93
Scenario 3	98.64	93.93	96.21	97.07	2.533	3.188	2.268	4.442
Scenario 4	98.78	88.35	95.69	97.96	2.34	2.172	2.324	5.808
Scenario 5	98.92	80.05	94.58	98.81	3.27	2.22	2.634	26.86
Scenario 6	80.85	87.52	91.59	84.73	0.802	4.293	3.309	1.163
Scenario 7	85.24	87.44	92.14	89.36	1.185	7.397	5.794	5.014
Scenario 8	87.21	87.29	92.58	92.08	1.812	10.539	8.623	25.331

TABLE 5. Average elapsed time of the methods.

	3DHT-MHT	PHD [3]+ Distance [3]	PHD [3]+ ART[6]	3DHT-TBD [9]
Scenario 1	28.8	18.92	25.41	24.35
Scenario 2	28.42	135.16	27.3	23.92
Scenario 3	28.29	151.74	27.65	23.77
Scenario 4	51.56	255.36	49.62	42.38
Scenario 5	99.51	538.62	68.17	79.93
Scenario 6	20.87	58.66	23.25	18.01
Scenario 7	42.1	130.64	43.92	35.44
Scenario 8	89.29	252.1	64.24	72.61

The computation of the method is also significant because a frame of measurements should be processed within a radar scanning cycle. The average running time of the 4 methods is patched in table 5. As a whole, more points (Scenario 5 and 8) means more computation. The computation of the 3DHT-MHT and 3DHT-TBD is proportional to the quantity of points. The computation of the integration of the PHD filter and distance partition method has exponential growth with a linear increase of points. Therefore, its running time is observably larger than the others in (Scenario 4, 5, 7and 8). But beyond that, the elapsed time of the others are similar**.**

Meanwhile. the performance of PHD filters is also related to the value of parameters. The parameters, such as the measurement rate and false alarm rate, have been set to fit the synthetic data of each scenario in simulation. The tracking performance would be deteriorated for inappropriate parameters.

B. REAL DATA

To demonstrate the proposed algorithm on a real-world application, 3DHT-MHT is tested using an air surveillance radar in a general airport. The real tracks of the targets are obtained by GPS (Global Positioning System) in the airplane. Two scenarios are presented in figure 7a and figure 7b, each scenario has two trajectories. The two targets are maneuvering or close in some scans. The measurements of the two scenarios are presented in figure 7c and figure 7d. The measurement rate of the airplane is time-varying and no measurements are generated by the airplane in some scans. For example, in scenario 2, the target 2 generates no measurements in 40 to 60 seconds. Figure 7e and figure 7g showcase the tracklets obtained by the 3DHT. Quite a few tracklets are generated around the real trajectories. Some false tracklets are also randomly built for clutter. The trajectories obtained by the 3DHT-MHT are presented in figure 7g and figure 7h. The two targets in scenario 1 have been well detected. In scenario 2, two shorter trajectories are obtained in figure 7h, rather than the integrated trajectory of target 2 in figure 7b. It mainly because no measurements are generated by the target 2 in these scans. Meanwhile, it is worth noting that no false alarm trajectories are built.

It is worth noting that the initial state of the target has also been given in the PHD filters. Actually, accurate values of the measurement rate and clutter rate are unknown. To achieve a better performance, parameters of the PHD filters are different in the two scenarios to achieve their optimal result. The OSPA distance of the two real scenarios is presented in figure 8. Figure 8 infers that the OSPA distance of the 3DHT-MHT is lower than the others in the majority of scans.

The average detection rate, the average false alarm number and the average OSPA distance of the two real scenarios are patched in table 6. The OSPA distance of the 3DHT-MHT is far less than the others because the high detection rate and no false trajectories. For instance, figure 7h infers that, both the weak tracklets originate from the targets and clutter are obtained for the low detection threshold in the first stage. In the other three methods, the false alarm trajectories would increase rapidly if such a low detection threshold is utilized to achieve a preferable detection rate. In scenario 2, the high false alarm number of 3DHT-TBD sharply decrease its performance, although an acceptable detection rate is reached for a lower detection threshold. The three state-of-arts are hard to overcome this dilemma. However, figure 7h presents that isolated tracklets would be abandoned in stage 2. This is

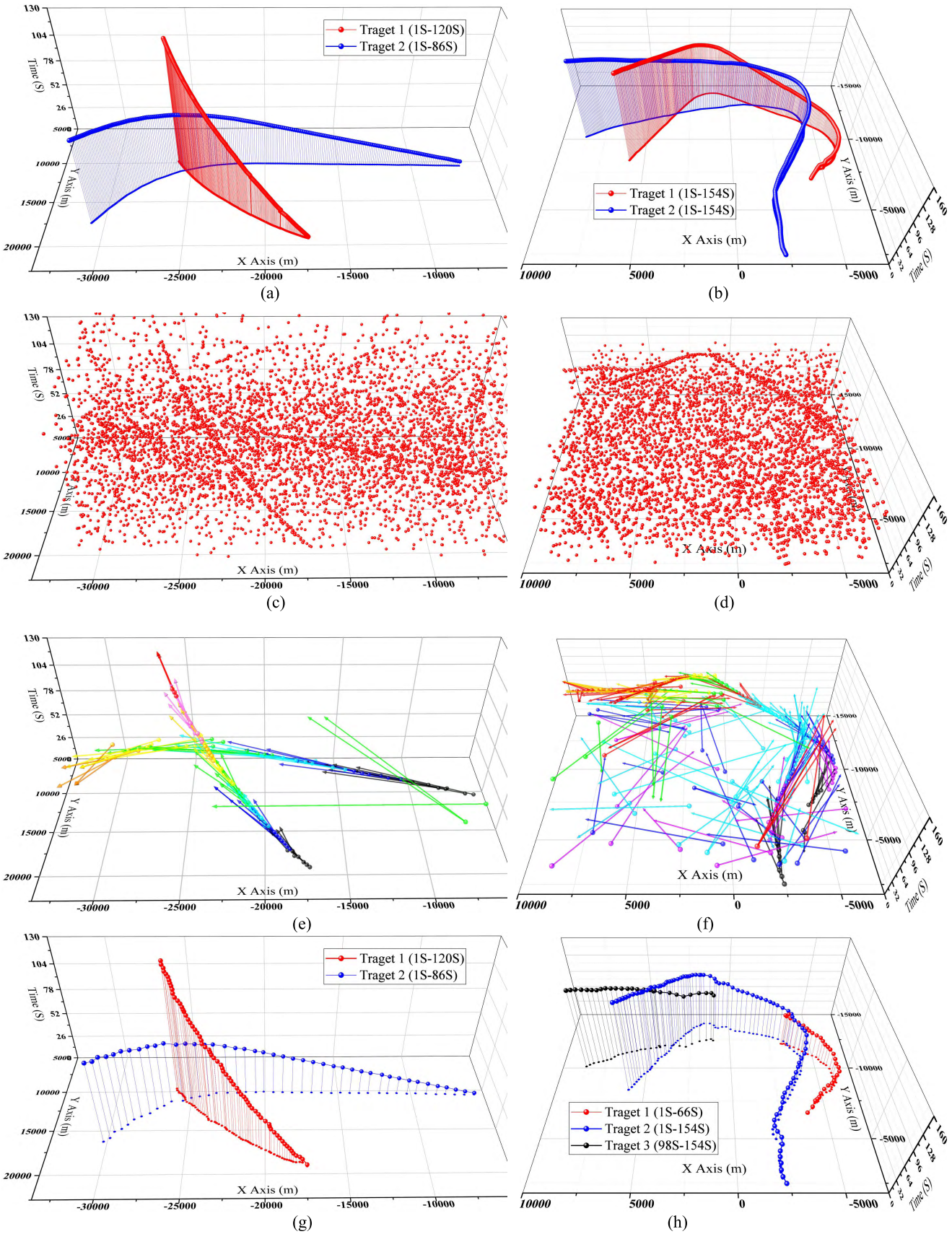

FIGURE 7. (a) The ground truth of two trajectories in scenario 1. (b) The ground truth of two trajectories in scenario 2. (c) The measurements of scenario 1. (d) The measurements of scenario 2. (e) The tracklets obtained by 3DHT in scenario 1. (f) The tracklets obtained by 3DHT in scenario 2. (g) The trajectories obtained by 3DHT-MHT in scenario 1. (h) The trajectories obtained by 3DHT-MHT in scenario.

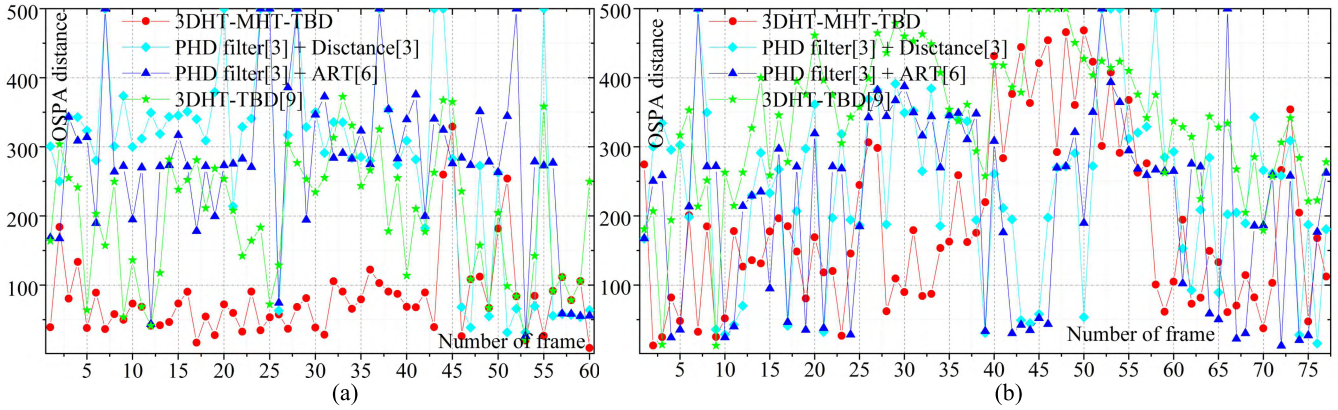

FIGURE 8. (a) The OSPA distance of scenario 1. (b) The OSPA distance of scenario 2.

TABLE 6. Results of the approaches.

	Scenario 1				Scenario 2			
	Detection rate of target 1	Detection rate of target2	False alarm number	OSPA distance	Detection rate of target 1	Detection rate of target2	False alarm number	OSPA distance
3DHT-MHT	100.00%	100%	0	80.94	80.52%	100.00%	0	138.32
PHD [3]+ Distance [3]	81.67%	74.89%	1.63	283.19	74.03%	85.71%	1.22	241.45
PHD [3]+ ART [6]	88.33%	83.97%	1.6	277.03	80.52%	96.10%	1.44	217.51
3DHT-TBD [9]	95.00%	95.32%	0.38	199.38	75.32%	81.82%	3	340.13

the precise reason why the proposed method can achieve a remarkable detection ability and suppressing clutter ability at the same time. Meanwhile, this is exactly the reason why the proposed method has a far lower OSPA distance.

V. CONCLUSION

In this article, the 3DHT and MHT were implemented to track and detect multiple weak and maneuvering extended targets in a radar system. The proposed method is able to find the optimal trajectories by the points in multiple scans. The method is superior to the existing methods especially when the extended target is weak or maneuvering. The 3DHT-TBD can not work well when the target is maneuvering because it is designed to detect straight lines. The PHD filter based methods are hard to detect the weak targets because merely the points in the current scan are utilized. Meanwhile, two merits of the 3DHT-MHT make it more practical in application. Firstly, the computation of the method is moderate in various scenarios. Secondly, far fewer parameters are necessary to be set. Therefore, the 3DHT-MHT is also available in various scenarios, especially in the scenario where the parameters are unknown.

APPENDIX

See Table 7.

TABLE 7. Parameters of the radar.

Parameter	Value
3 dB azimuth beam width	1.17°
Angular Precision	0.0439°
Range Resolution	24(m)
Number of range bin	8192
Scanning cycle of radar	2(s)
Rotating speed of antenna	180(°/s)

REFERENCES

[1] D. Musicki and R. J. Evans, "Multiscan multitarget tracking in clutter with integrated track splitting filter," *IEEE Trans. Aerosp. Electron. Syst.*, vol. 45, no. 4, pp. 1432–1447, Oct. 2009.

[2] C. Dalitz, T. Schramke, and M. Jeltsch, "Iterative Hough transform for line detection in 3D point clouds," *IEEE Trans. Image Process.*, vol. 7, pp. 184–196, Jul. 2017.

[3] K. Granström, C. Lundquist, and U. Orguner, "Extended target tracking using a Gaussian-mixture PHD filter," *IEEE Trans. Aerosp. Electron. Syst.*, vol. 48, no. 4, pp. 3268–3286, Oct. 2012.

[4] K. Granstrom and U. Orguner, "On spawning and combination of extended/group targets modeled with random matrices," *IEEE Trans. Signal Process.*, vol. 61, no. 3, pp. 678–692, Feb. 2013.

[5] R. Mahler, "PHD filters for nonstandard targets, I: Extended targets," in *Proc. 12th Int. Conf. Inf. Fusion*, Seattle, WA, USA, Jul. 2009, pp. 915–921.

[6] Y. Zhang and H. Ji, "A robust and fast partitioning algorithm for extended target tracking using a Gaussian inverse Wishart PHD filter," *Knowl. Based Syst.*, vol. 95, no. 1, pp. 125–141, Mar. 2016.
[7] T. Zhang and R. Wu, "Affinity propagation clustering of measurements for multiple extended target tracking," *Sensors*, vol. 15, no. 9, pp. 22646–22659, Sep. 2015.
[8] B. Yan, N. Xu, L. P. Xu, M. Q. Li, and P. Cheng, "An improved partitioning algorithm based on FCM algorithm for extended target tracking in PHD filter," *Digit. Signal Process.*, vol. 90, pp. 54–70, Jul. 2019.
[9] B. Yan, N. Xu, W.-B. Zhao, and L.-P. Xu, "A three-dimensional Hough transform-based track-before-detect technique for detecting extended targets in strong clutter backgrounds," *Sensors*, vol. 19, no. 4, p. 881, Feb. 2019.
[10] B. Sobhani, T. Zwick, and M. Chiani, "Target TOA association with the Hough transform in UWB radars," *IEEE Trans. Aerosp. Electron. Syst.*, vol. 52, no. 2, pp. 743–754, Apr. 2016.
[11] S. Mirjalili, S. Mohammad, and A. Lewis, "Grey wolf optimizer," *Adv. Eng. Softw.*, vol. 69, pp. 46–61, Mar. 2014.
[12] B. Yan, X. Y. Zhao, N. Xu, Y. Chen, and W. B. Zhao, "A grey wolf optimization-based track-before-detect method for maneuvering extended target detection and tracking," *Sensors*, vol. 19, no. 7, p. 1577, Mar. 2019.
[13] G. Wang, J. Xin, N. Zheng, and A. Sano, "Computationally efficient subspace-based method for two-dimensional direction estimation with L-shaped array," *IEEE Trans. Signal Process.*, vol. 59, no. 7, pp. 3197–3212, Jul. 2011.
[14] G. Wang, J. Xin, J. Wang, N. Zheng, and A. Sano, "Subspace-based two-dimensional direction estimation and tracking of multiple targets," *IEEE Trans. Aerosp. Electron. Syst.*, vol. 51, no. 2, pp. 1386–1402, Apr. 2014.
[15] T. L. Song, H. W. Kim, and D. Musicki, "Iterative joint integrated probabilistic data association for multitarget tracking," *IEEE Trans. Aerosp. Electron. Syst.*, vol. 51, no. 1, pp. 642–653, Jan. 2015.
[16] S. Puranik and J. K. Tugnait, "Tracking of multiple maneuvering targets using multiscan JPDA and IMM filtering," *IEEE Trans. Aerosp. Electron. Syst.*, vol. 43, no. 1, pp. 23–35, Jan. 2007.
[17] S. S. Blackman, "Multiple hypothesis tracking for multiple target tracking," *IEEE Aerosp. Electron. Syst. Mag.*, vol. 19, no. 1, pp. 5–18, Jan. 2004.
[18] A. Frank, P. Smyth, and A. Ihler, "Beyond MAP estimation with the track-oriented multiple hypothesis tracker," *IEEE Trans. Signal Process.*, vol. 62, no. 9, pp. 2413–2423, May 2014.
[19] K. Granström, N. Antonio, P. Braca, G. Ludeno, and F. Serafino, "Gamma Gaussian inverse Wishart probability hypothesis density for extended target tracking using X-band marine radar data," *IEEE Trans. Geosci. Remote Sens.*, vol. 53, no. 12, pp. 6617–6631, Dec. 2015.
[20] R.-L. Zhang, W.-X. Sheng, X.-F. Ma, and Y.-B. Han, "Clutter map CFAR detector based on maximal resolution cell," *Signal Image Video Process.*, vol. 9, no. 5, pp. 1151–1162, Jul. 2015.
[21] M. Chiani, A. Giorgetti, and E. Paolini, "Sensor radar for object tracking," *Proc. IEEE*, vol. 106, no. 6, pp. 1022–1041, Jun. 2018.
[22] K. Gilholm, S. Godsill, and S. Maskell, "Poisson models for extended target and group tracking," *Proc. SPIE*, San Diego, California, USA, vol. 5913, Sep. 2005, Art. no. 59130R.
[23] Q. Hu, H. Ji, and Y. Zhang, "A standard PHD filter for joint tracking and classification of maneuvering extended targets using random matrix," *Signal Process.*, vol. 144, pp. 352–363, Mar. 2018.
[24] R. D. Palkki, A. D. Lanterman, and W. D. Blair, "Addressing track hypothesis coalescence in sequential κ-best multiple hypothesis tracking," *IEEE Trans. Aerosp. Electron. Syst.*, vol. 47, no. 3, pp. 1551–1563, Jul. 2011.
[25] S. He, H. S. Shin, and A. Tsourdos, "Track-oriented multiple hypothesis tracking based on tabu search and Gibbs sampling," *IEEE Sensors J.*, vol. 18, no. 1, pp. 328–339, Jan. 2018.
[26] A. K. Gupta and D. K. Nagar, *Matrix Variate Distributions*. London, U.K.: Chapman-Hall, 2000.
[27] N. Nadarajah, R. Tharmarasa, M. McDonald, and T. Kirubarajan, "IMM forward filtering and backward smoothing for maneuvering target tracking," *IEEE Trans. Aerosp. Electron. Syst.*, vol. 48, no. 3, pp. 2673–2678, Jul. 2012.
[28] B.-T. Vo, D. Clark, B.-N. Vo, and B. Ristic, "Bernoulli forward-backward smoothing for joint target detection and tracking," *IEEE Trans. Signal Process.*, vol. 59, no. 9, pp. 4473–4477, Sep. 2011.
[29] B. Ristic, B.-N. Vo, and D. Clark, "Performance evaluation of multi-target tracking using the OSPA metric," in *Proc. 13th Int. Conf. Inf. Fusion*, Edinburgh, U.K., Jul. 2010, pp. 1–7.

BO YAN received the B.S. degree in communication engineering from Northwest University, Xi'an, China, in 2013, and the Ph.D. degree in guidance navigation and control from Xidian University, Xi'an, in 2018. He is currently with Xidian University. His research interests include radar data processing, multi-target detection and tracking, and data fusion.

NA XU was born in Xi'an, China, in 1994. She received the B.S. degree in communication engineering from Xidian University, Xi'an, in 2015, where she is currently pursuing the Ph.D. degree. Her research interests include radar signal processing and communication.

GUANGMIN WANG was born in Sichuan, China, in 1985. He received the B.E. degree in information and communication engineering and the Ph.D. degree in control science and engineering from Xi'an Jiaotong University, Xi'an, China, in 2008 and 2014, respectively. He is currently with Xidian University. His research interests include the areas of adaptive filtering, statistical and array signal processing, and pattern recognition.

SHENG YANG was born in Shanxi, China, in 1994. He received the B.S. degree in weapons systems and engineering from the North University of China, Taiyuan, China, in 2017. He is currently pursuing the M.D. degree with Xidian University. His research interests include radar target detection and tracking.

L. P. XU received the M.S. and Ph.D. degrees from Xidian University, in 1986 and 1996, respectively.

He became a Full Professor at Xidian University, Shaanxi, China, in 2000, where he is currently the Chair of the College of Space Science and Technology, Institute of Navigation, Detection and Guidance. In the past ten years, he has undertaken and completed a series of national and ministerial scientific research projects on radar information processing systems. He has edited five textbooks. He has more than 100 publications. He holds more than 30 patents. His research interests include radar, navigation, and multitarget detection.